Thermal and Electronic Transport Properties of p-Type ZnSb*

P. J. SHAVER†‡ AND JOHN BLAIR
Department of Electrical Engineering, Massachusetts Institute of Technology, Cambridge, Massachusetts
(Received 27 July 1965)

Galvanomagnetic, thermoelectric, and thermal-conductivity measurements were made on single-crystal specimens of p-type ZnSb, which has the orthorhombic symmetry D_{2h}. A horizontal zone-recrystallization process with an antimony-rich molten zone was used to produce the single crystals. Copper doping was used to control the hole concentration. Methods are described for making electrical and thermal contacts to this material. The experimental measurements included electrical resistivity and Hall effect (77.3° to 325°K) and extensive magnetoresistance measurements at 77.3°K. Measurements of thermoelectric power and thermal conductivity were made along the principal axes of oriented single-crystal cubes at 0°C. Considerable anisotropy was measured in the electrical conductivity. It was found that $\sigma_c=1.5\ \sigma_a=2.5\ \sigma_b$, approximately. The Hall effect and the thermoelectric power α were found to be isotropic. A slight (12%) anisotropy was measured in the thermal conductivity κ. For thermoelectric applications, the highest figure of merit, $Z=\alpha^2\sigma/\kappa$, is obtained with thermal and electrical currents directed along the c-axis of the crystal. At 0°C, the maximum Z was found to be 0.74×10^{-3} $(°K)^{-1}$. The experimentally observed results of the galvanomagnetic measurements are shown to be in agreement with a model for the electrical conduction processes which assumes that the valence band is composed of a single valley which is parabolic in $\mathbf{k}$ and has general ellipsoids for surfaces of constant energy. This model also assumes a relaxation time which is either a scalar function of energy or a diagonal tensor with a factorable energy dependence.

I. INTRODUCTION

THE primary purpose of this work is to investigate the electronic transport properties of p-type ZnSb by means of standard galvanomagnetic measurements. Measurements were made on carefully oriented single-crystal specimens. The measurements included electrical resistivity and Hall effect (77.3° to 325°K) and extensive magnetoresistance measurements at 77.3°K. Measurements of thermoelectric power and thermal conductivity were made along the principal axes of oriented single-crystal cubes at 0°C. This was done in order to evaluate the figure of merit for thermoelectric applications, $Z=\alpha^2\sigma/\kappa$.

The experimentally observed results of the galvanomagnetic measurements are shown to be in good agreement with a simple model for the valence-band conduction processes. This model assumes that a single general ellipsoid describes surfaces of constant energy in reciprocal space, that hole energy is a quadratic function of $\mathbf{k}$ and that a relaxation time exists which is either a scalar function of energy or a tensor that is diagonal in the principal coordinate system of the effective mass and has a factorable energy dependence.

The organization of this paper is as follows: Section II surveys past work on ZnSb. Section III presents the independent transport tensor coefficients (up through fourth order in $\mathbf{B}$) for the orthorhombic point group D_{2h}, outlines the measurement program and briefly describes the measurement instrumentation. Section IV describes the growth of ZnSb single crystals, the cutting of measurement samples and the electrical and thermal contact technology. Section V describes the results of the experimental measurements. Section VI interprets the results of the experimental measurements in terms of a theoretical model for the valence-band conduction processes. Section VII summarizes the results of this work. Appendix I presents theoretical expressions for the galvanomagnetic transport coefficients of a single general ellipsoidal, parabolic energy band, and Appendix II shows that the longitudinal magnetoresistance can vanish for this type of energy band for an arbitrary experimental orientation of the electric current.

II. SUMMARY OF PAST WORK

Zinc antimonide has long been of interest for use as the p-type leg of thermoelectric couples used for electrical power generation. Many of the previous investigations into ZnSb have been empirical optimizations of the performance of polycrystalline specimens in thermoelectric applications.[1,2] ZnSb-CdSb alloy systems have also been investigated in this context.[3] A number of investigations into the properties of single crystals of

* This work was supported by the National Aeronautics and Space Administration under Contract: NASA Grant NsG 496 (part).
† Now at the General Electric Research Laboratory, Schenectady, New York.
‡ Based in part on this author's dissertation presented to the Massachusetts Institute of Technology in partial fulfillment of the requirements of the degree of Doctor of Science, 1965.

[1] P. H. Egli, Inst. Radio Engrs. Trans. Mil. Electron. **6**, 27 (1962); M. Telkes, J. Appl. Phys. **18**, 1116 (1947); M. Telkes, *ibid.* **25**, 765 (1954); E. Justi and G. Schneider, Z. Naturforsch. **16a**, 628 (1961); O. V. Emeljanenko, E. Justi, and G. Schneider, *ibid.* **16a**, 1108 (1961).
[2] M. Telkes, Transactions of the Conference on the Use of Solar Energy, University of Arizona, Tucson, 1955 (unpublished).
[3] E. Justi and G. Neumann, U. S. Patent No. 3021378, 1962. E. Justi, in *Proceedings of the International Conference on Semiconductor Physics, 1960* (Czechoslovakian Academy of Sciences, Prague, 1961), p. 1074; M. Miksovsky, K. Smirous, and K. Toman, *ibid.*, p. 1087; L. Stourac, J. Tauc, and M. Zavetova, *ibid.*, p. 1091. I. M. Pilat, L. D. Shizh, and S. I. Voityshen, Zh. Tekhn. Fiz. **28**, 786 (1958) [English transl.: Soviet Phys.—Tech. Phys. **3**, 734 (1958)]. I. M. Pilat, G. S. Borodinets, L. A. Kosyachenko, and V. I. Maiko, Fiz. Tverd. Tela **2**, 1522 (1960) [English transl.: Soviet Phys.—Solid State **2**, 1381 (1961)].

ZnSb have been reported. Kot and Kretsu produced the first large crystals of ZnSb and later reported[4] measurements of electrical conductivities, Hall coefficients and thermoelectric powers on undoped, p-type single crystals. Although an attempt was made to investigate the possible anisotropy in the above quantities, the measurement samples had unknown absolute orientations. Eisner, Mazelsky, and Tiller,[5] Silvey, Lyons, and Silvestry,[6] and Hruby, Berankova, and Miskova[7] have described the preparation of undoped ZnSb single crystals by either the Czochralski or horizontal zone-recrystallization techniques. Little work was done on physical measurements. In 1964, Justi, Rasch, and Schneider[8] described the preparation of undoped and copper-doped, p-type ZnSb single crystals by the horizontal zone-recrystallization technique. Results were presented for thermoelectric power as a function of electrical conductivity and for the Hall effect, electrical conductivity and transverse magnetoresistance as functions of temperature between room temperature and 1.9°K. It was found that the $\alpha^2\sigma$ product for p-type ZnSb single crystals was significantly greater than that of polycrystalline ZnSb. Unfortunately, this work makes no mention of the crystallographic orientation of the measurement samples. Thus, the anisotropies of the electrical and thermal properties were not determined. In the same year, Komiya, Masumoto, and Fan[9] published the results of optical-absorption studies on oriented, undoped single-crystal samples of ZnSb. Absorption-edge energy thresholds of 0.50 eV (300°K), 0.59 eV (77°K) and 0.61 eV (4.2°K) were obtained independent of the direction of light polarization. Some evidence for an indirect energy gap was noted. Some data on the temperature dependence (77° to 340°K) and anisotropy of the Hall mobilities was included. Several other papers generally support the results presented in the work mentioned above.[10] Stevenson[11] has reported the observation of a single cyclotron resonance peak in p-type ZnSb. He did not determine the sign of the charge carrier and cites evidence for electrons' possibly being responsible for the observed resonance. Hirayama[12] has studied the thermal dissociation of ZnSb and identified zinc as the volatile species. Hansen[13] has presented a phase diagram for the Sb-Zn binary system. Hruby and Kaspar[14] have described chemical etches for ZnSb single crystal surfaces. Boltaks[15] has presented some values for the diffusion coefficients of tin and antimony in polycrystalline ZnSb. Frost *et al.*,[16] have briefly mentioned some effects of nuclear radiation on the electrical conductivity of polycrystalline ZnSb. X-ray investigations into the crystal structure of ZnSb and conjectures about possible atomic bonding schemes have been presented by a number of workers.[17] Khartsiev has made a group-theoretical investigation of the required symmetries of the electronic energy bands of ZnSb and the isomorphous compound CdSb.[18] Frei and Velitski[19] have criticized some of the analogies that Khartsiev drew in his work.

III. OUTLINE OF MEASUREMENTS

A. Number of Independent Transport Coefficients in the D_{2h} Point Group

It is of interest to note that gallium, TiO_2, cadmium antimonide and materials with the olivine crystal structure have the same macroscopic symmetry as zinc antimonide. This orthorhombic symmetry is characterized by the D_{2h} point group. The pertinent symmetry properties are[20] three mutually perpendicular, twofold rotation axes and a center of inversion. Applying these symmetry operations to the phenomenological expansions of quantities of experimental interest yields the following nonzero, independent elements for the various transport tensors (or pseudotensors, as the individual case may be):

Thermal conductivity:

$$\dot{Q}_i = -\sum_j \kappa_{ij} \nabla_j T \qquad \text{(III.1)}$$

$\kappa_{11}, \kappa_{22}, \kappa_{33}$ W/cm °K.

Thermoelectric power:

$$E_i = \sum_j \alpha_{ij} \nabla_j T \qquad \text{(III.2)}$$

$\alpha_{11}, \alpha_{22}, \alpha_{33}$ V/°K.

Electric-field strength as a function of magnetic-field

[4] M. V. Kot and I. V. Kretsu, Fiz. Tverd. Tela **2**, 1250 (1960) [English transl.: Soviet Phys.—Solid State **2**, 1134 (1960)].
[5] R. L. Eisner, R. Mazelsky, and W. A. Tiller, J. Appl. Phys. **32**, 1833 (1961).
[6] G. A. Silvey, V. J. Lyons, and V. J. Silvestri, J. Electrochem. Soc. **108**, 653 (1961).
[7] A. Hruby, J. Berankova, and V. Miskova, Phys. Status Solidi **3**, 289 (1963).
[8] E. Justi, W. Rasch, and G. Schneider, Advan. Energy Conversion **4**, 27 (1964).
[9] H. Komiya, K. Masumoto, and H. Y. Fan, Phys. Rev. **133**, A1679 (1964).
[10] M. Zavetova, Phys. Status Solidi **5**, K19 (1964); W. J. Turner, A. S. Fischler, and W. E. Reese, Phys. Rev. **121**, 759 (1961); W. J. Turner, A. S. Fischler, and W. E. Reese, J. Appl. Phys. **32**, 2241 (1961).
[11] M. J. Stevenson, *Proceedings of the International Conference on Semiconductor Physics, 1960* (Czechoslovakian Academy of Sciences, Prague, 1961), p. 1083.
[12] C. Hirayama, J. Electrochem. Soc. **110**, 80 (1963).
[13] M. Hansen, *Constitution of Binary Alloys* (McGraw-Hill Book Company, Inc., New York, 1958), p. 1185.
[14] A. Hruby and J. Kaspar, Czech. J. Phys. **12**, 799 (1962).
[15] B. I. Boltaks, *Diffusion in Semiconductors* (Academic Press Inc., New York, 1963), p. 304.
[16] R. T. Frost, J. C. Corelli, and M. Balicki, Advan. Energy Conversion **2**, 77 (1962).
[17] F. L. Carter and R. Mazelsky, J. Phys. Chem. Solids **25**, 571 (1964); Y. A. Ugai *et al.*, Zh. Strukt. Khim. **4**, 250 (1963); B. Velicky and V. Frei, Czech. J. Phys. **13**, 594 (1963); K. Toman, J. Phys. Chem. Solids **16**, 160 (1960); K. E. Almin, Acta Chem. Scandinavia **2**, 400 (1948).
[18] V. E. Khartsiev, Fiz. Tverd. Tela **4**, 983 (1961) [English transl.: Soviet Phys.—Solid State **4**, 721 (1962)].
[19] V. Frei and B. Velitski, Fiz. Tverd. Tela **5**, 962 (1963) [English transl.: Soviet Phys.—Solid State **5**, 706 (1963)].
[20] J. F. Nye, *Physical Properties of Crystals* (Oxford University Press, London, 1960), p. 284.

strength B_i and electric current density J_i:

$$E_i=J_i(\rho_{ii}+\rho_{iiii}B_i^2+\rho_{iijj}B_j^2+\rho_{iikk}B_k^2)+J_j(\rho_{ijk}B_k+2\rho_{ijij}B_iB_j)+J_k(\rho_{ikj}B_j+2\rho_{ikik}B_iB_k), \quad \text{(III.3a)}$$

with the following higher order terms (through fourth order in B)

$$+J_i(\rho_{iiiiii}B_i^4+\rho_{iijjjj}B_j^4+\rho_{iikkkk}B_k^4+6\rho_{iiiijj}B_i^2B_j^2+6\rho_{iiiikk}B_i^2B_k^2+6\rho_{iijjkk}B_j^2B_k^2)$$
$$+J_j(\rho_{ijkkk}B_k^3+3\rho_{ijiik}B_i^2B_k+3\rho_{ijjjk}B_j^2B_k+4\rho_{ijiiij}B_i^3B_j+4\rho_{ijijjj}B_iB_j^3+12\rho_{ijijkk}B_iB_jB_k^2)$$
$$+J_k(\rho_{ikjjj}B_j^3+3\rho_{ikiij}B_i^2B_j+3\rho_{ikjkk}B_jB_k^2+4\rho_{ikikkk}B_iB_k^3+4\rho_{ikiiik}B_i^3B_k+12\rho_{ikijjk}B_iB_j^2B_k). \quad \text{(III.3b)}$$

Here, $\dot{Q}_i$ is a component of a heat flux density (W/cm²), κ_{ij} is an element of the thermal-conductivity tensor, ∇_jT is a component of the temperature gradient (°K/cm), E_i is a component of the electric field (V/cm), α_{ij} is an element of the thermoelectric power tensor, J_i is a component of the electric current density (A/cm²), and B_i is a component of the magnetic flux density (kG).

In Eqs. (III.3a) and (III.3b), the literal subscripts mean that the components are to be assigned according to the following list of permutations:

i	j	k
1	2	3
2	3	1
3	1	2

Equations (III.3a) and (III.3b) are essentially just low-field expansions of the electrical resistivity, $\rho_{ij}(\mathbf{B})$, in terms of the magnetic flux density $\mathbf{B}$. These expressions include the additional symmetry required by the Onsager relationship: $\rho_{ij}(+\mathbf{B})=\rho_{ji}(-\mathbf{B})$. The nonzero tensor elements contained in Eq. (III.3a) can be conventionally identified as

Zero-magnetic-field electrical resistivity:

$$\rho_{11},\ \rho_{22},\ \rho_{33} \quad \Omega\ \text{cm}.$$

Hall coefficients:

$$\rho_{123}=-\rho_{213} \quad \text{cm}^3\ (\text{C})^{-1},$$
$$\rho_{312}=-\rho_{132},$$
$$\rho_{231}=-\rho_{321}.$$

Magnetoresistance coefficients:

$$\rho_{1111}\ \ \rho_{2211}\ \ \rho_{3311}\ \ \rho_{1212}$$
$$\rho_{1122}\ \ \rho_{2222}\ \ \rho_{3322}\ \ \rho_{1313} \quad (\Omega\ \text{cm})\ (\text{kG})^{-2}$$
$$\rho_{1133}\ \ \rho_{2233}\ \ \rho_{3333}\ \ \rho_{2323}.$$

The above results hold when the crystal is referred to its principal crystallographic axis coordinate system. The followlng convention is used to label the ZnSb crystal axes:

$$1=\langle 100\rangle=a=6.20\ \text{Å},$$
$$2=\langle 010\rangle=b=7.74\ \text{Å},$$
$$3=\langle 001\rangle=c=8.10\ \text{Å}.$$

In summary, it is seen that 3 thermal conductivities, 3 thermoelectric powers, 3 electrical resistivities, 3 Hall coefficients and 12 magnetoresistance coefficients need to be measured to completely characterize these particular transport properties.

B. Sample Geometries and Measured Coefficients

Thermal conductivity, thermoelectric power and electrical resistivity (by a two-terminal method) were measured on the same samples. These thermal samples were single-crystal rectangular parallelepipeds which were bounded by the three principal crystallographic coordinate planes. They measured 3 to 5 mm on a side. In general, κ_{ii}, α_{ii}, and ρ_{ii} were measured in each of the three principal directions on the same parallelepiped by suitably remounting it after one set of measurements was complete.

The galvanomagnetic samples were cut in the shape of rectangular bars generally 7 to 11 times longer than the largest transverse dimension which was 1.0 to 1.5 mm. As shown in Fig. 1(a), the same Hall coefficient could be measured twice as a check on sample homogeneity. It is obvious that the contact geometry of Fig. 1(a) will yield one electrical resistivity, one Hall coefficient and two magnetoresistance coefficients (e.g., ρ_{11}, ρ_{213}, ρ_{1111}, ρ_{1133}) when the current axis is mounted horizontally and one additional magnetoresistance coefficient with the current axis mounted vertically (e.g., ρ_{1122}). It is also possible to measure one of the "planar Hall coefficients"[21] (e.g., ρ_{2121}) by suitably remounting the same measurement sample. Thus, in principle, measurements on 3 galvanomagnetic samples are required to experimentally determine all 12 magneto-

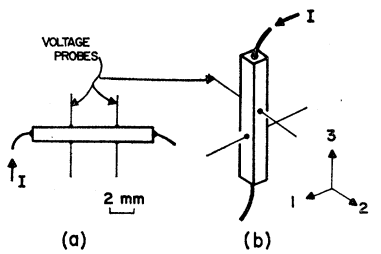

FIG. 1. Galvanomagnetic sample geometries. The standard geometry (a) was used to measure electrical resistivity, Hall effect, and magnetoresistance. Hall-coefficient anisotropy was measured on samples of type (b). In this case, ρ_{132} and ρ_{231} can be measured.

[21] A. C. Beer, *Galvanomagnetic Effects in Semiconductors* (Academic Press Inc., New York, 1963), p. 69.

resistance coefficients, 3 Hall coefficients and 3 electrical resistivities. Each of the three sample bars should have a different principal crystallographic direction as a current axis. In practice, due to the very small magnitude of the magnetoresistance measured in ZnSb, the "planar Hall coefficients" (e.g., ρ_{2121}) were not measured directly. Their values were inferred from longitudinal magnetoresistance measurements on single crystal bars that were cut so that their longitudinal axis (current axis) did not coincide with a principal crystallographic direction.

The sample geometry of Fig. 1(b) was used to measure the anisotropy in the Hall coefficient. With the current axis mounted vertically, two of the three independent Hall coefficients could be measured by simply rotating the sample holder by 90° (e.g., measure ρ_{132} and ρ_{231}). A second Hall sample, with a different current axis, could then be used to obtain both the remaining independent Hall coefficient and a second determination of one of the previously measured coefficients as a homogeneity check (e.g., ρ_{123} and $\rho_{321}=-\rho_{231}$ which was measured on the previous sample).

C. Description of Measurement Instrumentation

Thermal conductivity was measured by the familiar steady-state, absolute method. A low-temperature solder was used to attach the thermal sample to an electrical-resistance-heated copper block heat source and a copper block heat sink. The use of a low-freezing-point solder ($T_{\text{freezing}}<29.8$°C) minimized the mechanical strains and sample breakage due to differential thermal expansion between the anisotropic crystal, the heat source, and the heat sink. The heat sink was kept at 0°C during the course of measurement. The entire measurement assembly was kept in an evacuated chamber and was in thermal contact with an ice and water bath. The actual thermal power supplied to the thermal-conductivity sample in the steady state was computed by subtracting the previously calibrated heater losses (about 5% of the total input power) from the total electrical power input to the heater. The thermal conductivity was then computed using the known sample dimensions and the measured temperature difference. Temperature differences were generally kept between 1.5° and 4°C. Thermoelectric power was measured simultaneously by using the copper leads of the copper-constantan temperature-monitoring thermocouples as voltage probes. The electrical conductivity of the thermal sample was measured with a dc circuit that contained the sample as a two-terminal resistor. The resulting measured electrical conductivities agreed well with those that were measured on galvanomagnetic samples (operated as four terminal resistors). All voltages were measured with a Leeds and Northrup Type K-3 potentiometer.

Galvanomagnetic measurements were made with an ac measurement system. An ac sample current, a dc magnetic field, and a frequency-selective ac voltmeter were used. The use of frequencies above roughly 10 cps effectively eliminated the spurious influence of both Peltier heat generation at the current contacts and the Ettingshausen effect. The $\mathbf{B}=0$ voltage due to misalignment of the Hall probes and the $\mathbf{B}=0$ resistive voltage drop measured at the magnetoresistance probes were respectively nulled out with a cancellation voltage. This cancellation voltage was derived directly from the sample current. It was adjusted to proper amplitude and phase by suitable resistive and resistor-capacitor networks. With $\mathbf{B}\neq 0$, the resulting Hall or magnetoresistance voltage was read directly with a frequency-selective ac voltmeter that consisted of a Tektronix Type 122A battery-operated preamplifier and a General Radio Company Type 736-A wave analyzer. The galvanomagnetic sample was tied to the plane platform of an anodized aluminum sample holder. The electrical leads to the sample were carefully cemented to the sample holder in order to prevent vibration in the magnetic field. Measurements were made at a number of frequencies between 20 and 400 cps in order to insure the absence of spurious frequency effects. The sample holder was provided with an aluminum cover which completed the electrical, optical, and thermal shielding of the sample. Dip-stick measurements were made at the temperature of liquid nitrogen (77.3°K). Measurements of the Hall effect and electrical resistivity as a function of temperature were made as the sample holder drifted up towards room temperature as the liquid nitrogen in the Dewar evaporated. A small heater was used to reach temperatures that were slightly above room temperature. The temperature of the sample holder was monitored with a copper-constantan thermocouple which had been subjected to suitable calibration checks.

D. Measurements Made

To summarize, thermal conductivity, thermoelectric power, and electrical conductivity were all measured at 0°C. These measurements were confined to this temperature to avoid mechanical damage caused by the anisotropy in the differential thermal expansions of the crystal and the copper heat sink. These measurements were made on samples that had doping levels that varied from about 3×10^{16} (undoped) to 1×10^{19} holes/cm^3.

Measurements of electrical conductivities and Hall coefficients were made between 77.3°K and about 325°K on samples that had a variety of doping levels from about 3×10^{16} holes/cm^3 to 1×10^{19} holes/cm^3. The degree of anisotropy in the Hall effect was carefully checked at 77.3°K and room temperature at two doping levels. Extensive magnetoresistance measurements were made at 77.3°K at a doping level of about 4×10^{17} holes/cm^3. At room temperature and in the maximum available magnetic field, 12.5 (kG), the magnetoresistance was generally less than 0.02% ($p\approx3\times10^{16}$ cm^{-3}) which was too small to measure easily with the equipment and techniques used.

IV. CRYSTAL GROWTH AND SAMPLE PREPARATION

ZnSb forms by a peritectic reaction from a stoichiometric melt. Hence, it is difficult to prepare large single crystals by the usual crystal-growing techniques. The binary phase diagram[13] indicates that single crystals can be grown from an antimony-rich melt which has its liquidus temperature between the peritectic temperature, 546°C, and the eutectic temperature of 505°C. The method used to produce the ZnSb crystals used in this work was the horizontal zone-recrystallization technique that has been described by Kot and Kretsu[4] and Eisner, Mazelsky, and Tiller.[5] The molten zone used in the present work contained about a 5 at.% excess of antimony. The crystal-growth charges were contained in 15-mm-i.d. quartz ampoules that had been triply carbonized by the pyrolytic decomposition of acetone and subsequently outgassed at 800°C under vacuum. The growth charge consisted of three components: a single-crystal seed, a zone-leveling ingot that contained the excess antimony, and a nominally stoichiometric bulk ingot. The zone-leveling ingot and the bulk stoichiometric ingot were vacuum-melted, water-quenched alloy ingots. After the assembled crystal-growth charges were outgassed under vacuum (temperatures of 150° to 200°C, pressures $<10^{-5}$ Torr), the growth ampoule was filled with argon gas (one atmosphere absolute pressure at room temperature) and then sealed off from the vacuum system. The argon backfill was needed to suppress the serious decomposition of solid ZnSb that was encountered during the crystal-growth process in evacuated ampoules.

The crystals were grown in a horizontal zone furnace with an ambient temperature of 425°C and a nominal zone temperature of 580°C. The temperature gradient at the freezing interface was of the order of 60°C/cm. The molten zone was moved at a speed of about 0.030 in./hour. Care was taken to avoid subjecting large single crystals of ZnSb to sudden temperature changes. This was done in order to avoid thermal cracking of the brittle crystals. The resulting single crystals were about 7 mm thick, 10–15 cm long, and weighed on the order of 60 g. Early crystals were grown approximately along the ⟨001⟩ direction. These crystals were grown in uncarbonized quartz ampoules and often developed a number of low-angle grain boundaries (angles on the order of 0.2°) parallel to the growth direction, ⟨001⟩. Using carbonized quartz ampoules and growing along the ⟨316⟩ direction greatly reduced the occurrence of low-angle grain boundary formation. Boundaries that did form continued to lie nearly parallel to the ⟨001⟩ direction.

The resulting single-crystal ingots were checked for electrical uniformity by measuring longitudinal profiles of electrical conductivity and thermoelectric power with a four-point probe and a hot probe, respectively. Both the doped and undoped crystals were found to be electrically uniform to within at least ±5%.

Doped crystals were grown by adding the chemical impurity to the antimony-rich zone-leveling charge. The stoichiometric-alloy portion of the growth charge was undoped. Aluminum-, selenium-, and indium-doped crystals were grown in attempts to produce n-type ZnSb. These attempts were unsuccessful. These crystals still exhibited p-type conductivity as was evidenced by the sign of the thermoelectric power measured with a hot probe at room temperature. Justi *et al.*[8] have tried tellurium and gallium doping in unsuccessful attempts to produce n-type ZnSb.

The crystal ingots were cut by the spark-erosion cutting technique.[22] The crystals were too brittle to be cut reliably with the diamond-grit rotary cut-off wheels which were available for use in this investigation. Spark-erosion cutting conditions were adjusted to give cutting speeds of about 1 cm/h. It was possible to cut at much higher rates, but not without danger of producing thermally induced crack damage in the crystals which possibly was due to intense local heating near the spark-erosion cutting zone.

Electrical contacts were made with ordinary lead-tin solder applied to freshly sandblasted surfaces with a rosin flux. Copper wire, with a diameter of 1.5 mils, was used for voltage probes. The diameter of the solder dots at the voltage-probe contacts was of the order of 0.1 mm. These contacts were Ohmic (at 77.3 and 300°K) up to current densities of 50 A/cm², which was the highest current level tested.

Thermal contacts were made by using gallium as a low-temperature solder (melting point of 29.8°C). The appropriate faces of the approximately cube-shaped thermal-conductivity sample were carefully plated with indium from an indium sulfamate plating solution.[23] The indium-plated faces were then tinned with gallium. The proper surfaces of the copper heat source and sink were also tinned with gallium. The appropriate surfaces were then mated and the gallium solder was frozen as the temperature of the thermal conductivity apparatus was cooled down towards 0°C. This low-temperature soldering technique minimized crystal breakage caused by differential thermal expansion between the crystal faces and the copper heat source and sink. A thermal sample could be easily removed from the apparatus and the residual contact material dissolved off in concentrated HCl. Thus, it was possible to make thermal conductivity measurements along the three principal crystallographic axes of the same cube. These contacts were found to have negligible thermal resistance and were electrically Ohmic up to current densities of 0.5 A/cm², which was the highest current density tested.

With few exceptions, all galvanomagnetic and thermal

[22] H. H. Ehlers and D. F. Kolesar, Tech. Rept. No. 303, MIT Lincoln Laboratories, 1963 (unpublished).

[23] Indium Corporation of America, 1676 Lincoln Ave., Utica, New York.

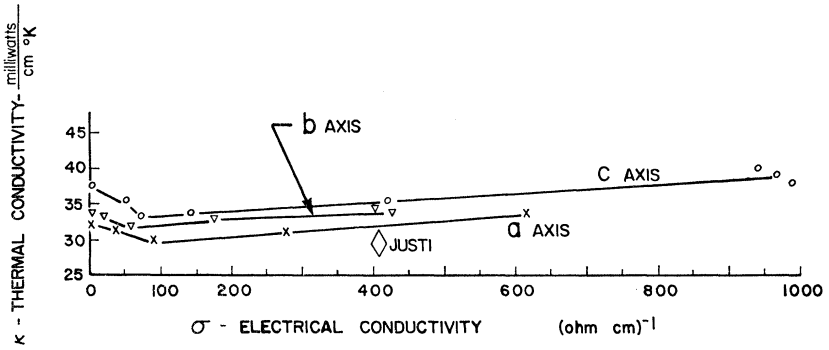

FIG. 2. Thermal conductivity versus electrical conductivity, p-type ZnSb at 0°C. Datum point from Justi *et al.* (see Ref. 8) is a room-temperature measurement on a sample of unspecified orientation.

measurement samples had sandblasted surfaces. Experimental checks indicated that chemically etching the sample surfaces had no effect on the results of any galvanomagnetic measurement.

V. EXPERIMENTAL RESULTS

A. Thermal Measurements

Annealing Experiments

Several previous investigators[4,9,10] have reported that the electrical properties of ZnSb apparently change with time when measurements are made at high temperatures. The hole concentration apparently increases with increasing ambient temperature. This effect has been observed in this work also. Undoped single crystals were annealed in nitrogen or argon atmospheres at temperatures up to 240°C. The hole concentration p measured at room temperature by means of the Hall effect was found to increase with annealing temperature. A plot of $\ln p$ versus T^{-1} could be approximated by a straight line of slope 1.0 eV. At room temperature, the equilibrium hole density was of the order of 2×10^{16} cm^{-3}. When the annealed samples were stored at room temperature, their hole concentrations would gradually decrease towards the original, room-temperature value. Plots of $[p(t=0)-p(t)]\times[p(t=0)-p(t=\infty)]^{-1}$, where t is time and $t=0$ corresponds to the moment that the sample temperature is decreased to end the annealing cycle, yield a short time behavior proportional to $t^{2/3}$ and a long-term behavior similar to $[1-\exp(Kt)]$ where K is an appropriate negative constant. The asymptotic behavior of a number of these recovery curves seemed to indicate that complete recovery (to within a few percent of the equilibrium room temperature value) would be obtained in 1000 to 10 000 h time—depending upon the particular annealing sample. This type of behavior was noted on 13 samples that were cut from four different undoped crystals. The presence or absence of electrical contacts during annealing seemed to have no direct effect on the results. Sandblasting fresh surfaces on annealed crystals had no effect on the observed changes in hole concentration. Thus, this reversible change in carrier concentration is not primarily a contact or a surface effect. The basic mechanism may be similar to the observed precipitation of Te and Pb on dislocations in PbTe crystals.[24] Further experimental work, including a correlation of the shape of the recovery curves with observed crystal dislocation densities is needed before a definite explanation can be advanced for these phenomena in ZnSb.

Thermal-Conductivity Measurement

The results of the thermal conductivity measurements at 0°C are shown as Fig. 2. The estimated probable errors are $\pm3\%$ for the electrical conductivity and $\pm4\%$ for the thermal conductivity. There is about a 12% maximum anisotropy in the thermal conductivities. It seems reasonable to numerically order them as: $\kappa_{33}>\kappa_{22}>\kappa_{11}$. Evidently, almost the entire amounts of the observed thermal conductivities are due to the lattice (phonon) component. Because of the large lattice component of heat conduction, it is not possible to reliably estimate Lorenz numbers for hole conduction from this data.

Thermoelectric-Power Measurement

Figure 3 presents the measured thermoelectric powers as a function of electrical conductivity at 0°C. The estimated probable errors are $\pm3\%$ for both the thermoelectric power and the electrical conductivity. The thermoelectric power is evidently isotropic for p-type ZnSb. Also shown on this figure are the data points of Justi *et al.*,[8] for single crystals and polycrystals of ZnSb. Their measurements were probably made at room temperature. No orientations were reported for their single-crystal specimens.

Figure of Merit for Thermoelectric Applications

Owing to the large anisotropy in the electrical conductivity, it is clear from Fig. 3 that operation along the c axis of a ZnSb crystal will give the highest thermoelectric figure of merit, $Z=\alpha_{ii}^2\sigma_{ii}/\kappa_{ii}$. Here α_{ii} is the thermoelectric power, σ_{ii} is the electrical conductivity and κ_{ii} is the thermal conductivity along the ith principal axis of the crystal. The c-axis thermoelectric-power

[24] W. W. Scanlon, Phys. Rev. 126, **509** (1962).

data have the following analytical representation:

$$\alpha_{33}=795-210\log_{10}\sigma_{33},$$

where α is given in μV/°K and σ has the units of $(\Omega\ \text{cm})^{-1}$. The maximum of $\alpha^2\sigma$ can be found by differentiation. At 0°C, the resultant maximum in $\alpha^2\sigma$ occurs at $\sigma_{33}=825$ $(\Omega\ \text{cm})^{-1}$ and is equal to 2.74×10^{-5} $W/\text{cm}\ °\text{K}^2$. The thermal-conductivity data indicate that $\kappa_{33}=0.037$ $W/\text{cm}\ °\text{K}$ at this electrical-conductivity level. The thermal conductivity is not very sharply dependent upon the electrical conductivity in this range. Thus, for p-type ZnSb single crystals at 0°C, $Z_{\max}=0.74\times10^{-3}°\text{K}^{-1}$ and occurs when the thermal and electrical currents are directed along the c axis of the crystal. This is a figure of merit which is nearly the same as that obtained with heavily doped polycrystalline material at room temperature[25] even though the thermal conductivity of the single crystals is appreciably greater than values which have been quoted for polycrystalline material. These values range from 0.013 to 0.026 W/cm °K at room temperature.[2,8,25]

B. Results of Galvanomagnetic Measurements

The annealing and recovery phenomena described above make it difficult to accurately determine the anisotropies in the electrical properties of undoped, p-type ZnSb. Extreme care must be exercised in order to insure that every measurement sample has exactly the same thermal history—both with regard to elapsed time after growth (ambient temperature=425°C) and any subsequent thermal cycling such as soldering operations or high temperature measurements. In this work, these difficulties were avoided by confining the bulk of the measurements to crystals that were heavily doped.

Taking no precaution regarding the thermal histories of undoped samples, measured hole concentrations fell

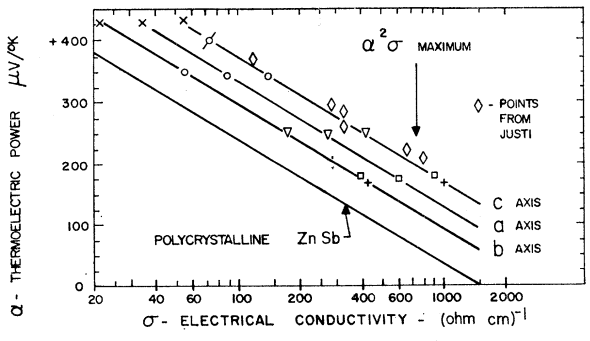

FIG. 3. Thermoelectric power versus electrical conductivity, p-type ZnSb at 0°C. Data points and the line for polycrystals are from Justi *et al.* (see Ref. 8) and are room-temperature measurements on samples of unspecified orientation. For the results of the present investigation, the same graphical symbol is used to mark the results obtained from successive measurements along the different axes of the same measurement sample.

[25] R. R. Heikes and R. W. Ure, *Thermoelectricity: Science and Engineering* (Interscience Publishers, Inc., New York, 1961), p. 406.

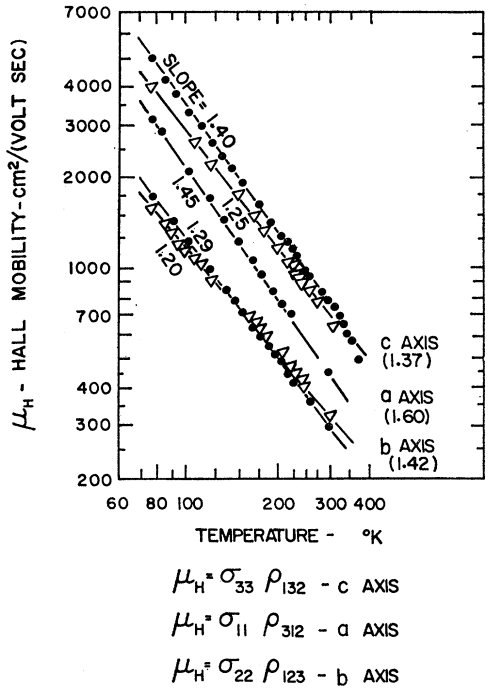

FIG. 4. Hall mobilities versus temperature, undoped p-type ZnSb. The numbers in parentheses are the slopes of the Hall-mobility curves of Komiya *et al.* (see Ref. 9).

in the range of 2 to 4×10^{16} cm^{-3}. Throughout this work, hole concentrations are approximated by $p\approx(q\rho_{ijk})^{-1}$ where q is the electronic charge. The scatter in the measured value for any one Hall coefficient (e.g., ρ_{132}) was as large as the measured differences in any two crystallographically independent Hall coefficients (e.g., ρ_{132} and ρ_{321}). As a result, only Hall mobilities for some undoped samples are presented in Fig. 4. The corresponding slopes from the data of Komiya *et al.*,[9] have been included for reference. The slopes are near the value of 1.5 expected for acoustic phonon scattering. The Hall effect and electrical resistivity data were similar to the a-axis data presented by Komiya *et al.*[9] The residual acceptor level responsible for the p-type conduction had an activation energy of about 4.6×10^{-3} eV. The variation in the slopes of the Hall mobility versus temperature curves is probably due to differences in the amount of ionized impurity scattering present in the various samples. The samples with lower carrier concentrations had slopes closer to 1.5. Figure 5 shows c-axis Hall mobilities versus temperature for crystals with four different hole concentrations. The influence of increasing ionized-impurity scattering is evident.

Extensive measurements were made on samples cut from a copper-doped crystal (number C-1078-C) that had a room-temperature hole concentration of 4×10^{17} cm^{-3}. This doping level decreased the importance of carrier density changes due to the previously mentioned annealing effects. A 1×10^{16} cm^{-3} change in hole density

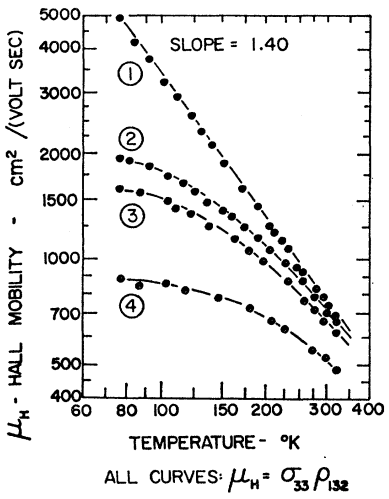

FIG. 5. Hall mobilities versus temperatures, p-type ZnSb at various hole concentrations, $p \approx (q\rho_{132})^{-1}$, at 273°K: Curve (1) 3×10^{16}, (2) 4×10^{17}, (3) 5.5×10^{17}, and (4) 1×10^{19} cm^{-3}.

—quite serious in an undoped crystal—amounts to only a 2.5% change in hole concentration at this doping level.

Figure 6 presents the results of measurements of the temperature variation of the electrical conductivity and two of the three independent Hall coefficients. Figure 7 presents the corresponding Hall mobilities. At this doping level, it is difficult to interpret the slope of the Hall-coefficient curves, which corresponds to an apparent activation energy of 0.9×10^{-3} eV. The impurity energy levels may be smeared over a finite range of

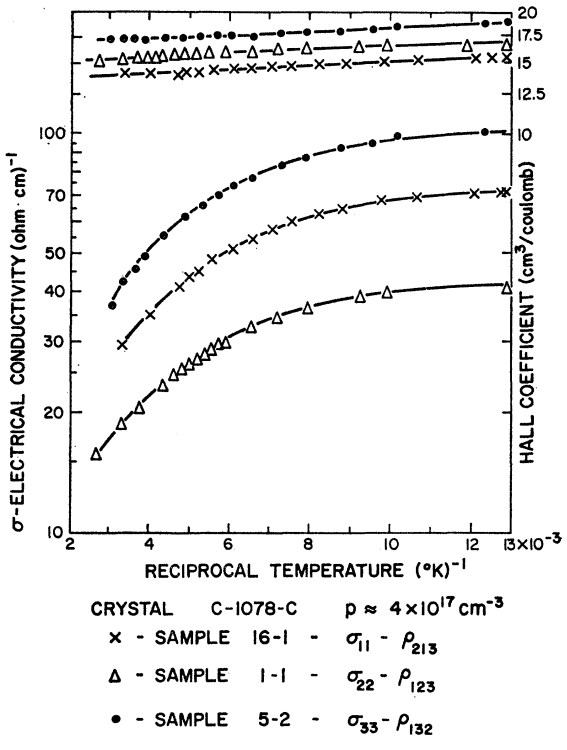

FIG. 6. Hall coefficient and electrical conductivity versus $(T)^{-1}$, copper-doped p-type ZnSb.

TABLE I. Measured Hall coefficients, in cm³/C—copper-doped ZnSb, sample geometry shown in Fig. 1(a).

Coefficient	Crystal C-1078-C, $p\approx4\times10^{17}$ cm^{-3} 300°K	77.3°K	
ρ_{123}, ρ_{213}	14.1±1	15.7±1	(4 samples)
ρ_{231}	14.0	16.5	(1 sample)
ρ_{132}, ρ_{312}	16.3±1	18.4±1.5	(6 samples)

energies. Onsager symmetry requires that $\rho_{123}=-\rho_{213}$. However, Fig. 6 shows an 8% difference between ρ_{123} and ρ_{213}. The estimated probable instrument error in the absolute value of a measured Hall coefficient is ±2%. It was found that values for the same Hall coefficient, when measured at different sets of contacts on the same sample, usually differed by no more than 3 to 5%. Thus, it is possible that a combination of instrument errors, sample inhomogeneities, and the perturbing influence of the finite size of the Hall-voltage probe solder contacts

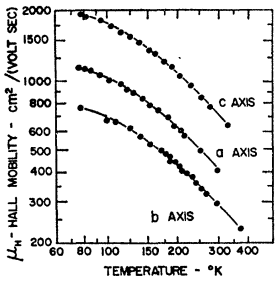

FIG. 7. Hall mobilities versus temperature, copper-doped, p-type ZnSb. These curves were computed from the data of Fig. 6.

(0.1-mm diam. on a sample 1.0 to 1.5 mm high) could lead to scatter as large as 8 or 10% in the measured Hall coefficients. As a result, these measurements of the Hall coefficient cannot be expected to reliably detect anisotropy in the Hall coefficients which is any smaller than 10%. Table I summarizes the results of Hall-coefficient measurements on samples cut from this particular copper-doped crystal. Arithmetic averages are given and the scatter in the measurement results indicated. Data for ρ_{ijk} and ρ_{jik} were averaged together. The ac voltmeter indicated only the magnitude of a

TABLE II. Measured Hall coefficients, in cm³/C—copper-doped ZnSb, sample geometry shown in Fig. 1(b).

	Crystal C-1073-B, $p\approx5.5\times10^{17}$ cm^{-3} 300°K	77.3°K	Sample number
ρ_{123}	11.9	12.9	1-1
ρ_{321}	10.5	11.4	1-1
ρ_{231}	11.6	13.2	2-1
ρ_{132}	11.0	12.2	2-1
	Crystal C-1075-B, $p\approx1\times10^{19}$ cm^{-3}		
ρ_{123}	0.594	0.609	1-1
ρ_{321}	0.576	0.593	1-1
ρ_{231}	0.550	0.560	2-1
ρ_{132}	0.568	0.570	2-1

galvanomagnetic voltage and not the algebraic sign. Table II indicates the results of Hall-effect measurements on two sets of samples of the geometry shown in Fig. 1(b). These measurements were made at hole concentrations of about 5.5×10^{17} and 1×10^{19} cm^{-3}, respectively. These tables indicate that the three independent Hall coefficients, ρ_{123}, ρ_{132}, and ρ_{231}, have magnitudes which are within at least $\pm10\%$ of being equal. Furthermore, these data do not indicate any consistent differences between the magnitudes of the three independent Hall coefficients. Thus, it seems reasonable to conclude that the Hall effect is isotropic in p-type ZnSb.

The magnetic field dependences of the measured Hall voltages were checked at room temperature and at 77.3°K, for magnetic fields between 200 G and 12.5 kG, and at approximate hole concentrations of 2×10^{16}, 4×10^{17}, 5.5×10^{17}, and 1×10^{19} cm^{-3}. The measured Hall voltages were linear in B, showing only an apparently nonsystematic $\pm2\%$ maximum deviation from a linear field dependence. These fluctuations are close to the estimated experimental accuracy of the measurement.

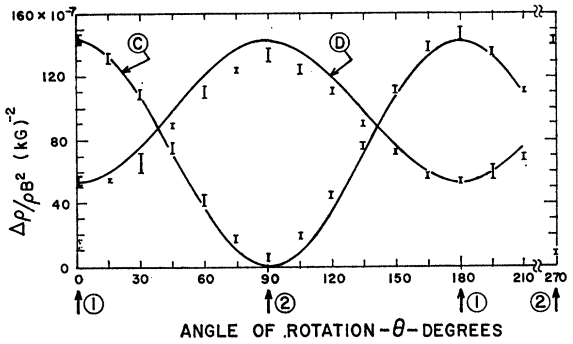

FIG. 8. Magnetoresistance in copper-doped p-type ZnSb at 77.3°K. $p\approx4\times10^{17}$ cm^{-3}. Electric current along the a axis. Curve (C), $143\times10^{-7}\cos^2\theta$: Brackets enclose data points for sample No. 15-1 and $B=12.5$, 11.0, 10.0, and 8.0 kG. **B** rotated in (001) plane. At orientation (1), measure ρ_{1122}/ρ_{11}. At orientation (2), measure ρ_{1111}/ρ_{11}. Curve (D), $53\times10^{-7}\cos^2\theta+143\times10^{-7}\sin^2\theta$: Brackets enclose data points for sample No. 16-1 and $B=12.5$ and 10.0 kG. **B** rotated in (100) plane. At orientation (1), measure ρ_{1133}/ρ_{11}. At orientation (2), measure ρ_{1122}/ρ_{11}.

Magnetoresistance was measured in undoped ($p\approx2\times10^{16}$ cm^{-3}) and copper-doped (crystal C-1078-C, $p\approx4\times10^{17}$ cm^{-3}) p-type ZnSb at liquid-nitrogen temperature for magnetic-field flux densities between 8 and 12.5 kG. At room temperature and in a 12.5-kG field, the magnetoresistance was of the order of 0.02% and less and was close to the limits of resolution of the instrumentation. At 77.3°K, the magnetoresistance voltage changes followed a simple B^2 magnetic field dependence to within $\pm5\%$. No systematic deviations from a B^2 behavior were ever observed. In some cases, using undoped samples, the magnetic-field dependence was checked down to levels as low as 1 kG with the same results. The absolute accuracy of the magnetoresistance measurement, $\Delta\rho/\rho B^2$, is estimated to be $\pm10\%$. This magnitude of probable error is mainly due to the fact that properly averaging the measured $+\mathbf{B}$ and $-\mathbf{B}$ magnetoresistance voltages to remove a spurious component due to the Hall effect often amounted to taking the difference of two large numbers. At 12.5 kG the electric field component which gives rise to the Hall voltage was found to be roughly two orders of magnitude larger than the change in the longitudinal component of the electric field caused by the magnetoresistance. Thus, slight departures from ideal galvanomagnetic sample geometry introduced a large Hall component into the measured magnetoresistance voltage.

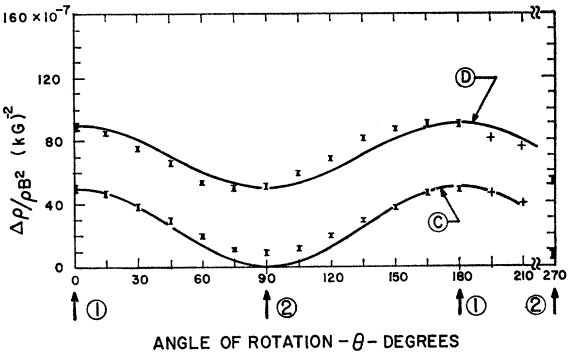

FIG. 9. Magnetoresistance in copper-doped, p-type ZnSb at 77.3°K. $p\approx4\times10^{17}$ cm^{-3}. Electric current along the b axis. Curve (C), $50\times10^{-7}\cos^2\theta$: Brackets enclose data points for sample No. 13-1 and $B=12.5$, 11.0, and 10.0 kG. **B** rotated in (100) plane. At orientation (1), measure ρ_{2233}/ρ_{22}. At orientation (2), measure ρ_{2222}/ρ_{22}. Curve (D), $90\times10^{-7}\cos^2\theta+50\times10^{-7}\sin^2\theta$: Brackets enclose data points for sample No. 12-1 and $B=12.5$, 11.0, and 10.0 kG. **B** rotated in (010) plane. At orientation (1), measure ρ_{2211}/ρ_{22}. At orientation (2), measure ρ_{2233}/ρ_{22}.

Only qualitative magnetoresistance measurements were made with undoped samples. The angular dependence of the magnetoresistance effect was of precisely the

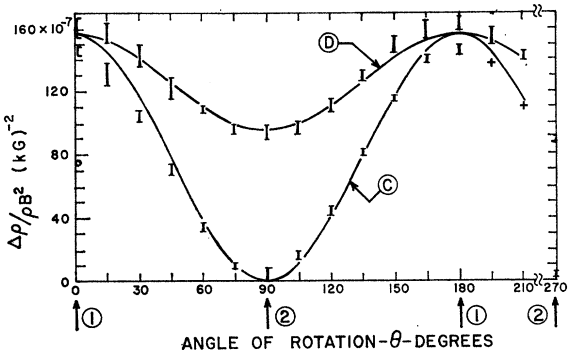

FIG. 10. Magnetoresistance in copper-doped, p-type ZnSb at 77.3°K. $p\approx4\times10^{17}$ cm^{-3}. Electric current along the c axis. Curve (C), $157\times10^{-7}\cos^2\theta$: Brackets enclose data points for sample No. 22-1 and $B=12.5$, 11.0, and 10.0 kG. **B** rotated in (100) plane. At orientation (1), measure ρ_{3322}/ρ_{33}. At orientation (2), measure ρ_{3333}/ρ_{33}. Curve (D), $157\times10^{-7}\cos^2\theta+95\times10^{-7}\sin^2\theta$: Brackets enclose data points for sample No. 5-1 and $B=12.5$, 11.0, and 10.0 kG. **B** rotated in (001) plane. At orientation (1), measure ρ_{3322}/ρ_{33}. At orientation (2), measure ρ_{3311}/ρ_{33}.

TABLE III. Measured galvanomagnetic coefficients for copper-doped p-type ZnSb.

Crystal C-1078-C 77.3°K $p \approx 4\times10^{17}$ cm^{-3}

$\rho_{11}=1.40(\pm0.10)\times10^{-2}$ (Ω cm)
$\rho_{22}=2.20(\pm0.15)\times10^{-2}$
$\rho_{33}=0.95(\pm0.07)\times10^{-2}$
$\rho_{123}=\rho_{312}=\rho_{231}=16.9\pm2.0$ cm^3/C

In units of (kG)$^{-2}$ and with a probable error of ±10%.

$\rho_{1111}/\rho_{11}\approx0$ (5.8×10^{-7})	$\rho_{2211}/\rho_{22}=90\times10^{-7}$	$\rho_{3311}/\rho_{33}=95\times10^{-7}$
$\rho_{1122}/\rho_{11}=143\times10^{-7}$	$\rho_{2222}/\rho_{22}\approx0$ (14×10^{-7})	$\rho_{3322}/\rho_{33}=157\times10^{-7}$
$\rho_{1133}/\rho_{11}=53\times10^{-7}$	$\rho_{2233}/\rho_{22}=50\times10^{-7}$	$\rho_{3333}/\rho_{33}\approx0$ (6.8×10^{-7})

$\rho_{1313}=-24(\pm6)\times10^{-9}$ (Ω cm)/(kG)^2.
$\rho_{1212}=-85(\pm9)\times10^{-9}$.
$\rho_{2323}=-65(\pm15)\times10^{-9}$. This value was not measured. It was inferred from other data.

same nature as that which was measured on the doped samples.

Figures 8, 9, and 10 present typical magnetoresistance results with the electric current density directed down the a, b, and c axes of samples cut from copper-doped crystal C-1078-C ($p\approx4\times10^{17}$ cm^{-3}). Brackets have been drawn that represent the total scatter for all of the data points that correspond to a given angle between the magnetic field and the electric current axis of the sample. These magnetoresistance results were reproducible to within 10% on two different sets of measurement samples cut from this crystal. The curves shown on these figures were drawn by using the numerical results of Table III for the transverse magnetoresistance coefficients. Qualitatively, Figs. 8, 9, and 10 indicate that the longitudinal magnetoresistance is close to vanishing with electric current directed along the a, b, and c axes of the crystal. A residual longitudinal magnetoresistance on the order of $\Delta\rho/\rho B^2=5$ to 10×10^{-7} (kG)$^{-2}$ was common to most of the measurement samples. This probably represents a residual effect[26]

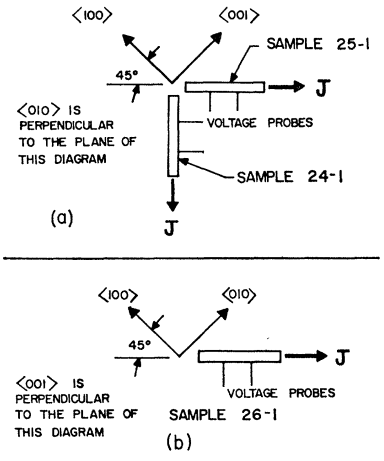

FIG. 11. Sample geometries for "off-axis" magnetoresistance measurements. (a) Shows samples cut from an (010) wafer. (b) Shows a sample cut from an (001) wafer. Measurement results for these samples appear in Fig. 12.

[26] A. C. Beer, Ref. 21, p. 308.

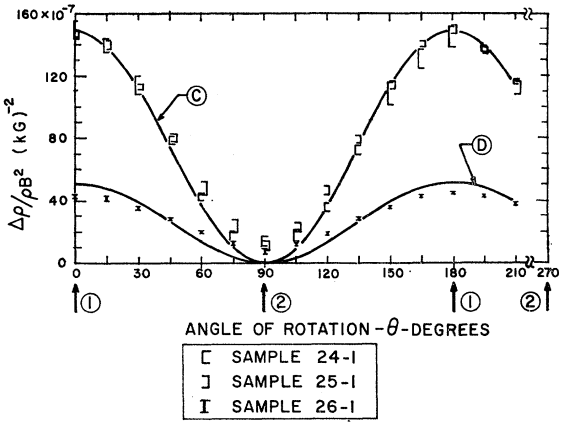

FIG. 12. Magnetoresistance measurements on the samples of Fig. 11. Copper-doped p-type ZnSb at 77.3°K. $p\approx4\times10^{17}$ cm^{-3}. Curve (C): for the model of Appendix II, the equation of the expected curve is: $\Delta\rho/\rho B^2=(\rho_{11}+\rho_{33})^{-1}(\rho_{1122}+\rho_{3322})\cos^2\theta$. Inserting numerical values from Table III yields: $\Delta\rho/\rho B^2=149\times10^{-7}\cos^2\theta$. Brackets enclose data points for samples 24-1 and 25-1 at magnetic field densities of $B=12.5$, 11.0, and 10.0 kG. At orientation (1), **B** is directed along the ⟨010⟩ direction. At orientation (2), **B** and **J** are parallel and longitudinal magnetoresistance is being measured. Curve (D): for the model of Appendix II, the equation of the expected curve is: $\Delta\rho/\rho B^2=(\rho_{11}+\rho_{22})^{-1}(\rho_{1133}+\rho_{2233})\cos^2\theta$. Inserting numerical values from Table III yields: $\Delta\rho/\rho B^2=51\times10^{-7}\cos^2\theta$. Brackets enclose data points for sample 26-1 and magnetic field densities of 12.5, 11.0, 10.0 kG. At orientation (1), **B** is directed along the ⟨001⟩ direction. At orientation (2), **B** and **J** are parallel and longitudinal magnetoresistance is being measured.

which is characteristic of the degree of electrical and mechanical perfection of both the crystal and the contact technology. This residual effect looks large on the b-axis data because of the relatively small magnitude of the transverse effect, ρ_{2233}/ρ_{22}. Chemically etching the surface of a b-axis sample had no effect on the measured magnetoresistance—the transverse value was unchanged and a longitudinal effect of a similar size was present. The same relative amount of residual longitudinal magnetoresistance was also obtained in measurements on undoped, b-axis samples.

Assuming that the valence band can be represented by one or more valleys which have general ellipsoids for constant energy surfaces, the observed vanishing longitudinal magnetoresistance along the a, b, and c crystallographic axes indicates that the valence-band ellipsoid system is arranged with the principal axes of the ellipsoids coincident with the a, b, and c axes. This is reminiscent of the conduction band structure of n-type silicon. Figure 11 shows the sample geometries and Fig. 12 shows the results of measurements on samples that were cut so that the current axes were at least 45° from any one of the three principal crystallographic axes. This type of measurement will be called an "off-axis" magnetoresistance measurement as contrasted to the "on-axis" results measured on samples that have **J** coincident with a principal crystallographic axis. These results indicate that the "off-axis" longitudinal magnetoresistance vanishes to within the same degree of approximation as the "on-axis" longitudinal magneto-

resistance results presented in Figs. 8, 9, and 10. This result may be somewhat unexpected. However, as is shown in Appendix II, this result is entirely consistent with the model for the valence-band conduction processes presented in the next section. The values of the so-called "planar Hall" coefficients, ρ_{2121}, ρ_{3131}, and ρ_{2323} can be calculated from data such as that shown in Fig. 12. For the data of curve (c), at $\theta=90°$ (longitudinal magnetoresistance),

$$\Delta\rho/\rho B^2=\tfrac{1}{2}(\rho_{11}+\rho_{33})^{-1}(\rho_{1133}+\rho_{3311}+4\rho_{3131}).$$

Since ρ_{11}, ρ_{33}, ρ_{1133}, and ρ_{3311} were measured on other samples, the above equation can be solved for ρ_{3131}. This procedure was used to experimentally determine ρ_{3131} and ρ_{2121}. A value for ρ_{2323} was not measured experimentally. However, ρ_{2323} can be estimated from an expression similar to the above and the assumption that the longitudinal magnetoresistance vanishes regardless of the orientation of **J** (refer to Appendix II for details).

The results of these galvanomagnetic measurements on this copper-doped, p-type ZnSb crystal are summarized in Table III. The numbers presented for the magnetoresistance coefficients are arithmetic averages of 6 or more experimental values. These values were obtained on two or more samples—the one exception being ρ_{2211}/ρ_{22} which was measured on just one sample. Several magnetic field levels in the range of 8 to 12.5 kG were also used. The maximum scatter observed in the experimental magnetoresistance results was 10%. An interesting numerical symmetry is evident in the magnetoresistance results. To within 10%: $\rho_{2211}/\rho_{22}=\rho_{3311}/\rho_{33}$, $\rho_{1122}/\rho_{11}=\rho_{3322}/\rho_{33}$, and $\rho_{1133}/\rho_{11}=\rho_{2233}/\rho_{22}$.

VI. MODEL FOR THE ZnSb VALENCE BAND

A model for the valence band conduction processes must explain the following experimental results: isotropic thermoelectric power, isotropic Hall effect, anisotropic electrical conductivity (**B**=0), vanishing longitudinal magnetoresistance with **J** parallel to a principal crystallographic axis ("on axis"), vanishing longitudinal magnetoresistance with **J** not parallel to a principal crystallographic axis ("off axis") and the numerical symmetry which has been observed in the transverse magnetoresistance results.

A simple valence band which exhibits the orthorhombic symmetry of the crystal lattice is a single valley, centered at **k**=0, which has a general ellipsoid as a surface of constant energy. This ellipsoid must have its principal axes parallel to the a, b, and c axes of the unit cell of the crystal in order to exhibit the required orthorhombic symmetry. It is assumed that the valley is parabolic, that is,

$$E(\mathbf{k})=\frac{\hbar^2}{2}\left(\frac{k_1^2}{m_{11}}+\frac{k_2^2}{m_{22}}+\frac{k_3^2}{m_{33}}\right),$$

where $E(\mathbf{k})$ is the energy of a hole which has reciprocal lattice vector **k** (with components k_1, k_2, k_3), and m_{11}, m_{22}, and m_{33} are the components of the effective mass tensor—which is diagonal in this coordinate system. This energy band—a single valley with constant energy surfaces in the form of general ellipsoids and a parabolic **k** dependence—will be called a SEP band in the following discussion. With the experimental measurements made in this work, there is no way of deciding whether just one valley or many *identically* oriented valleys are present. It is assumed that a tensor relaxation time exists. At a given temperature, its components are assumed to be a function of hole energy only. The relaxation time should have at least the symmetry of the crystal lattice and is therefore assumed to be diagonal in the same coordinate system as the effective mass. Stevenson[11] has reported a single cyclotron-resonance peak in p-type ZnSb at 1.5°K. The sign of the carrier (holes or electrons) which was responsible for the resonance was not determined. The data indicated an energy band with an ellipsoid of revolution for a surface of constant energy. The symmetry axis was the "a direction" of the crystal and the observed effective masses were: $m_t/m_0=0.146\pm0.010$ and $m_l/m_0=0.175\pm0.010$ where m_0 is the free electron mass. Since the carrier which was responsible for the resonance was not identified, the following analysis proceeds using a valence band which has a general ellipsoid instead of an ellipsoid of revolution for a constant energy surface. The ellipsoid of revolution is just a special case of this model.

The galvanomagnetic coefficients for a SEP valence band are developed in Appendix I. Any one of the following five forms can be used for the relaxation time:

A. An isotropic, constant relaxation time:

$$\tau_{ij}=\tau\delta_{ij}.$$

B. An anisotropic, constant relation time:

$$\tau_{ij}=\tau_i\delta_{ij}.$$

C. An isotropic function of energy:

$$\tau_{ij}=F(E)\delta_{ij}.$$

D. An anisotropic relaxation time with a factorable energy dependence:

$$\tau_{ij}=\tau_iF(E)\delta_{ij}.$$

E. An anisotropic relaxation time with an unfactorable energy dependence:

$$\tau_{ij}=\tau_i(E)\delta_{ij}.$$

In the above, E is the energy of a hole, $F(E)$ and $\tau_i(E)$ are functions of energy, δ_{ij} is the Kronecker delta symbol, and i, j range over the principal coordinate directions of 1, 2, and 3. These relaxation times will be referred to as forms "A," "B," etc., in the following. It is obvious that relaxation times forms A, B, C, and D are just special cases of form E. Finally, the following

energy average is defined:

$$\langle F(E)\rangle=-\frac{2}{3}\frac{\int_0^\infty F(E)E^{3/2}(\partial f^0/\partial E)dE}{\int_0^\infty E^{1/2}f^0dE}, \quad \text{(VI.1)}$$

where $F(E)$ is a function of energy and f^0 is the Fermi-Dirac distribution function. With this background in hand, the implications of the experimental results will now be considered.

Thermoelectric Power

Figure 3 indicates that the thermoelectric power of p-type ZnSb is isotropic to within the experimental accuracy of $\pm 3\%$. For a single general ellipsoid, the elements of the diagonal thermoelectric power tensor are given by[27]

$$\alpha_{ij}=\frac{1}{Tq}\frac{\langle(E-E_F)\tau_{ii}\rangle}{\langle\tau_{ii}\rangle}\delta_{ij}. \quad \text{(VI.2)}$$

Here, T is absolute temperature, and q is the hole charge, $+1.602\times10^{-19}$ C. It is seen that the thermoelectric power will be isotropic for relaxation times of the forms A, B, C, and D, but not E, in general.

Hall Effect

The results presented in Tables I and II indicate that the Hall effect is probably isotropic. The Hall coefficients have the form:

$$\rho_{ijk}=-\epsilon_{ijk}\frac{1}{pq}\frac{\langle\tau_{ii}\tau_{jj}\rangle}{\langle\tau_{ii}\rangle\langle\tau_{jj}\rangle}. \quad \text{(VI.3)}$$

Here, p is the hole density and $\epsilon_{123}=\epsilon_{312}=\epsilon_{231}=+1$, $\epsilon_{213}=\epsilon_{132}=\epsilon_{321}=-1$ and $\epsilon_{ijk}=0$ if any two indices are equal. It is seen that the Hall effect will be isotropic for relaxation times of the forms, A, B, C, and D, but not E, in general.

Electrical Conductivity at Zero Magnetic Field

Figure 3 and Table III indicate that $\sigma_{33}\approx1.5\sigma_{11}\approx2.5\sigma_{22}$. For a SEP valence band

$$\sigma_{ij}=(pq^2\langle\tau_{ii}\rangle/m_{ii})\delta_{ij}. \quad \text{(VI.4)}$$

[27] Since both the effective-mass and relaxation-time tensor have been assumed to be diagonal in the principal coordinate system of the orthorhombic crystal, this equation is a direct generalization of the usual expression for one dimensional thermoelectricity with an isotropic relaxation time (e.g., Heikes and Ure, Ref. 25, p. 52). The appropriate element of the diagonal relaxation-time tensor is used for each principal direction of the crystal as long as there is no applied magnetic field.

It is seen that the measured anisotropies can arise from anisotropies in the effective masses, the relaxation times, or a combination of both.

Magnetoresistance Results

For a SEP valence band, the "on-axis" longitudinal magnetoresistance coefficients, ρ_{1111}, ρ_{2222}, and ρ_{3333} are zero for all forms of the relaxation time considered—A through E. Furthermore, as is shown in Appendix II, the longitudinal magnetoresistance will vanish in an arbitrary direction (i.e., "off axis") for relaxation times of the form A through D, but not E. Actually, relaxation times of forms A and B are trivial in this context because they also give an identically zero transverse magnetoresistance.

A certain numerical symmetry has been observed in the transverse magnetoresistance results. Table III indicates that

$$\rho_{2211}/\rho_{22}=\rho_{3311}/\rho_{33},$$
$$\rho_{1122}/\rho_{11}=\rho_{3322}/\rho_{33},$$
$$\rho_{1133}/\rho_{11}=\rho_{2233}/\rho_{22}.$$

Using the results of Appendix I, the first of the observed numerical equalities requires that

$$\frac{pq^2\langle\tau_{22}\rangle}{m_{22}}\frac{1}{pm_{33}}\left[\frac{\langle\tau_{22}^2\tau_{33}\rangle}{\langle\tau_{22}\rangle^2}-\frac{\langle\tau_{22}\tau_{33}\rangle^2}{\langle\tau_{22}\rangle^2\langle\tau_{33}\rangle}\right]=\frac{pq^2\langle\tau_{33}\rangle}{m_{33}}\frac{1}{pm_{22}}\left[\frac{\langle\tau_{33}^2\tau_{22}\rangle}{\langle\tau_{33}\rangle^2}-\frac{\langle\tau_{33}\tau_{22}\rangle^2}{\langle\tau_{33}\rangle^2\langle\tau_{22}\rangle}\right], \quad \text{(VI.5)}$$

which reduces to

$$\langle\tau_{22}^2\tau_{33}\rangle\langle\tau_{33}\rangle=\langle\tau_{33}^2\tau_{22}\rangle\langle\tau_{22}\rangle. \quad \text{(VI.6a)}$$

Similarly the other two experimentally observed equalities require that

$$\langle\tau_{11}^2\tau_{22}\rangle\langle\tau_{22}\rangle=\langle\tau_{22}^2\tau_{11}\rangle\langle\tau_{11}\rangle \quad \text{(VI.6b)}$$

and

$$\langle\tau_{33}^2\tau_{11}\rangle\langle\tau_{11}\rangle=\langle\tau_{11}^2\tau_{33}\rangle\langle\tau_{33}\rangle. \quad \text{(VI.6c)}$$

Since relaxation times of the form A and B are discarded as being trivial, only relaxation times of the form C and D but not, in general, E will lead to the indicated numerical symmetry in the observed magnetoresistance results.

Further Discussion of the Valence-Band Model

In view of the above developments, the functional form of the relaxation time is either of form C, an isotropic function of energy, or of form D, an anisotropic relaxation time with a factorable energy dependence. Figure 5 indicates that both ionized impurity and acoustic phonon scattering are important at 77.3°K and at a doping level of $p\approx4\times10^{17}$ cm^{-3}. Assuming that the appropriate transition probabilities are additive, the

total relaxation time may be written as

$$(\tau_T)_{ii}^{-1}=(\tau_I)_{ii}^{-1}+(\tau_A)_{ii}^{-1}, \qquad \text{(VI.7)}$$

where $(\tau_T)_{ii}$ is a diagonal element of the total relaxation-time tensor and $(\tau_I)_{ii}$ and $(\tau_A)_{ii}$ are the corresponding elements of the ionized-impurity and acoustic-phonon relaxation-time tensors, respectively. If both $(\tau_I)_{ij}$ and $(\tau_A)_{ij}$ are isotropic, then $(\tau_T)_{ij}$ will be of form C. If $(\tau_I)_{ij}$ and $(\tau_A)_{ij}$ are individually of form D *and* exhibit the same relative anisotropy, then $(\tau_T)_{ij}$ will also be of form D. A choice between forms C and D cannot be made without further experimental information. This would include an unambiguous determination of the effective masses and, ideally, the additional parameters that are required by theories of charge carrier scattering —such as static dielectric constants, elastic constants and deformation potentials. For the rest of the discussion, a relaxation time of form D, $\tau_{ij}=\tau_i F(E)\delta_{ij}$, will be used. Form C is just a special case of form D and is obtained by setting $\tau_1=\tau_2=\tau_3$.

If this model for the ZnSb valence-band conduction processes is accurate, then the results of Appendix I can be used to show that the transverse magnetoresistance is

$$\frac{\rho_{iijj}}{\rho_{ii}}=\frac{q^2}{\beta_i\beta_k}\left[\frac{\langle F^3\rangle}{\langle F\rangle}-\frac{\langle F^2\rangle^2}{\langle F\rangle^2}\right], \qquad \text{(VI.8)}$$

that the Hall mobilities are

$$(\mu_H)_{ii}=(q/\beta_i)\langle F^2\rangle/\langle F\rangle, \qquad \text{(VI.9)}$$

and that the electrical conductivities are

$$\sigma_{ii}=(pq^2/\beta_i)\langle F\rangle, \qquad \text{(VI.10)}$$

where $i\neq j\neq k$ and range over the principal coordinate directions 1, 2, and 3. Also, $F=F(E)$ and a relaxation time of form D has been assumed.

In the above,

$$\beta_i=m_{ii}/\tau_i. \qquad \text{(VI.11)}$$

Notice that a direct check on the validity of the magnetoresistance results can now be made. Using the above expressions, it is seen that:

Ratio of transverse magnetoresistance coefficients:

$$(\rho_{iijj}/\rho_{ii})/(\rho_{iikk}/\rho_{ii})=\beta_j/\beta_k.$$

Ratio of Hall mobilities:

$$(\mu_H)_{kk}/(\mu_H)_{jj}=\beta_j/\beta_k.$$

Ratio of electrical conductivities:

$$(\sigma_{kk})/(\sigma_{jj})=\beta_j/\beta_k.$$

These ratios of experimentally measured quantities are presented in Table IV. Since six different transverse magnetoresistance coefficients were measured, three independent ratios of experimentally measured quantities can be formed. Furthermore, $(\beta_3/\beta_2)(\beta_2/\beta_1)(\beta_1/\beta_3)=1$.

TABLE IV. Comparison of magnetoresistance, Hall-mobility, and electrical-conductivity ratios. (All of the following quantities were measured experimentally.)

	β_3/β_2	β_2/β_1	β_1/β_3[a]
Magnetoresistance[b] ratios, $p\approx4\times10^{17}$ cm^{-3}, 77.3°K			
$(\rho_{1133}/\rho_{11})/(\rho_{1122}/\rho_{11})$	0.37		
$(\rho_{3322}/\rho_{33})/(\rho_{3311}/\rho_{33})$		1.65	
$(\rho_{2211}/\rho_{22})/(\rho_{2233}/\rho_{22})$			1.80
Hall mobility ratios			
$p\approx4\times10^{17}$ cm^{-3}, 77.3°K[c]	0.40	1.54	1.62
$p\approx4\times10^{17}$, 300°K[d]	0.39	1.49	1.74
$p\approx2\times10^{16}$, 273°K[e]	0.34	1.85	1.59
$p\approx2\times10^{16}$, 273°K[f]	0.40	1.58	1.60
Electrical conductivity ratios			
$p\approx1\times10^{19}$, 273°K[g]	0.39	1.66	1.55

[a] Except for the quoted magnetoresistance ratio, the numbers in this column are simply the ratios of the appropriate entries in the first two columns of the same row. As a result, the third column ratios are not independent of the ratios of the first two columns.
[b] Crystal C-1078-C, 77.3°K data presented in Table III.
[c] Crystal C-1078-C, 77.3°K data presented in Fig. 7.
[d] Crystal C-1078-C, 300°K data presented in Fig. 7.
[e] Data points read from Fig. 2 of Komiya, Masumoto, and Fan, Ref. 9. Undoped, p-type crystals.
[f] Crystal C-1081-C, 273°K data presented in Fig. 4. Undoped, p-type crystals.
[g] Crystal C-1075-B, 273°K. These results are typical of anisotropy data for $4\times10^{17}<p<1\times10^{19}$ presented in Fig. 3.

The product obtained with the experimental magnetoresistance ratios is 1.10, which is reasonably close to 1.00. In the case of experimentally measured Hall mobilities and electrical conductivities, the ratios in the third column of Table IV are not independent of the ratios of the first two columns. This is because only three independent, experimental quantities (e.g., σ_{11}, σ_{22}, and σ_{33}) were used to form three ratios. Since the magnetoresistance ratios have an estimated probable error of $\pm14\%$ and the Hall mobility and electrical conductivity ratios about $\pm7\%$, the agreement obtained in Table IV is good. The data taken from the work of Komiya *et al.*[9] are in reasonable agreement with the rest of the results presented in this table (see note "e" of Table IV). Table IV demonstrates the quantitative validity of the magnetoresistance measurement results —at least within the framework of the band structure and relaxation time model chosen for the valence band.

Using a measured thermoelectric power, a hole concentration obtained from Hall effect measurements (now including the $\langle\tau^2\rangle/\langle\tau\rangle^2=3\pi/8$ factor for acoustic phonon scattering) and an assumed form for the relaxation time, the density-of-states effective mass can be estimated. Using experimental results for crystal C-1078-C at 273°K and assuming that only acoustic phonon scattering is important, the value obtained is:

$$m_d=0.42m_0(\pm0.15m_0).$$

For a single general ellipsoid the density-of-states effective mass is:

$$m_d=(m_{11}m_{22}m_{33})^{1/3}.$$

Assuming that the relaxation time is isotropic, the

77.3°K magnetoresistance ratios of Table IV give

$$\beta_3/\beta_2=m_{33}/m_{22}=0.37 \quad \text{and} \quad \beta_2/\beta_1=m_{22}/m_{11}=1.65.$$

Combining these results yields the following, very approximate, estimates of the effective masses: $m_{11}=0.42m_0$, $m_{22}=0.69m_0$ and $m_{33}=0.26m_0$.

VII. SUMMARY

Galvanomagnetic, thermoelectric, and thermal-conductivity measurements were performed on oriented single crystal specimens of p-type ZnSb. These measurements indicate a slight (12%) anisotropy in the thermal conductivity at 0°C, no anisotropy in the thermoelectric power at 0°C, and no anisotropy in the Hall effect at 77.3° and 300°K. Considerable anisotropy was measured in the electrical conductivity. It was found that $\sigma_c=1.5\sigma_a=2.5\sigma_b$, approximately. For thermoelectric applications, the highest figure of merit is obtained with thermal and electrical currents directed along the c axis of the crystal. At 0°C, the maximum thermoelectric figure of merit was found to be 0.74×10^{-3} °K^{-1}. The thermal conductivity at this doping level was 0.037 W/cm °K. The experimentally observed results of the galvanomagnetic measurements are shown to be in excellent agreement with a model for the valence band conduction processes which assumes that the valence band is composed of a single valley which is parabolic in **k** and has general ellipsoids for surfaces of constant energy. The relaxation time is assumed to be either a scalar function of hole energy or a diagonal tensor with a factorable energy dependence.

ACKNOWLEDGMENTS

The authors would like to thank Professor A. C. Smith, Professor D. C. White, and Professor J. F. Janak for helpful comments made during the course of this work. William J. Brennan and Eric K. Li were of invaluable help in many experimental phases of this work. Professor R. E. Newnham, Dr. J. H. Fang, and R. Mills provided the x-ray facilities which were used to orient the crystals. K. J. Button, W. Tice, and E. Ferri made the facilities of the National Magnet Laboratory available for the spark-erosion cutting of the single crystals.

APPENDIX I: GALVANOMAGNETIC COEFFICIENTS FOR A GENERAL ELLIPSOID

Expressions will now be developed for the coefficients in the following phenomenological expansion of the electrical resistivity. In the limit of low magnetic flux densities:

$$\rho_{ij}(\mathbf{B})=\rho_{ij}+\sum_k \rho_{ijk}B_k+\sum_{k,l}\rho_{ijkl}B_kB_l.$$

The electrical conductivity is defined as

$$\sum_j \sigma_{ij}(\mathbf{B})\rho_{jk}(\mathbf{B})=\delta_{ik}.$$

Using a similar low-field expansion gives

$$\sigma_{ij}(\mathbf{B})=\sigma_{ij}+\sum_k \sigma_{ijk}B_k+\sum_{k,l}\sigma_{ijkl}B_kB_l.$$

From these three equations, it is seen that

$$\sum_j \sigma_{ij}\rho_{jk}=\delta_{ik}.$$

The Hall coefficients are

$$\rho_{lkp}=-\sum_{i,j}\rho_{li}\sigma_{ijp}\rho_{jk},$$

and the magnetoresistance coefficients are

$$\rho_{lkmn}=\tfrac{1}{2}\sum_{i,j,p,r}\rho_{li}\rho_{jp}\rho_{rk}[\sigma_{ijn}\sigma_{prm}+\sigma_{ijm}\sigma_{prn}]-\sum_{i,j}\rho_{li}\rho_{jk}\sigma_{ijmn}.$$

Herring and Vogt[28] have presented theoretical expressions for the conductivity coefficients of a SEP energy band. The relaxation time was assumed to be diagonal in the principal coordinate system of the energy band. The relaxation time was assumed to be a function of energy only, although each element of the diagonal tensor could be a different function of energy. This is the most general form of the valence band and relaxation time model considered in this present work. Their results can be written as:

Electrical conductivity:

$$\sigma_{ij}=(pq^2/m_{ii})\langle\tau_{ii}\rangle\delta_{ij}.$$

"Hall" conductivity:

$$\sigma_{ijk}=(pq^3/m_{ii}m_{jj})\langle\tau_{ii}\tau_{jj}\rangle\epsilon_{ijk}.$$

Magnetoconductivity:

$$\sigma_{ijkl}=(pq^4/m_{ii}m_{jj})\sum_f\frac{1}{2m_{ff}}(\epsilon_{ikf}\epsilon_{flj}+\epsilon_{ilf}\epsilon_{fkj})\langle\tau_{ii}\tau_{jj}\tau_{ff}\rangle,$$

where the energy average, $\langle F(E)\rangle$, for a function of energy, $F(E)$, has been defined in Eq. (VI.1). In the above expressions, p is the volume density of holes, q is the electric charge of a hole ($+1.602\times10^{-19}$ C) and ϵ_{ijk} is the permutation symbol which has been defined in the text.

Using the above inversion formulas, the following expressions are obtained for the galvanomagnetic coefficients:

Electrical resistivities ($\mathbf{B}=0$):

$$\rho_{ij}=(m_{ii}/pq^2\langle\tau_{ii}\rangle)\delta_{ij} \quad (\Omega\ \text{m}). \tag{A1}$$

Hall coefficients:

$$\rho_{ijk}=-\frac{1}{pq}\frac{\langle\tau_{ii}\tau_{jj}\rangle}{\langle\tau_{ii}\rangle\langle\tau_{jj}\rangle}\epsilon_{ijk} \quad (\text{m}^3/\text{C}). \tag{A2}$$

[28] C. Herring and E. Vogt, Phys. Rev. **101**, 944 (1956).

Magnetoresistance coefficients:

$$\rho_{iiii}=0 \quad (\Omega\ \mathrm{m}^5)/\mathrm{Wb}^2, \tag{A3a}$$

$$\rho_{iijj}=\frac{1}{pm_{kk}}\left[\frac{\langle\tau_{ii}^2\tau_{kk}\rangle}{\langle\tau_{ii}\rangle^2}-\frac{\langle\tau_{ii}\tau_{kk}\rangle^2}{\langle\tau_{ii}\rangle^2\langle\tau_{kk}\rangle}\right], \tag{A3b}$$

$$\rho_{ijij}=-\frac{1}{2pm_{kk}}\left[\frac{\langle\tau_{ii}\tau_{jj}\tau_{kk}\rangle}{\langle\tau_{ii}\rangle\langle\tau_{jj}\rangle}-\frac{\langle\tau_{ii}\tau_{kk}\rangle\langle\tau_{jj}\tau_{kk}\rangle}{\langle\tau_{ii}\rangle\langle\tau_{jj}\rangle\langle\tau_{kk}\rangle}\right]. \tag{A3c}$$

Unless required by the Kronecker delta, δ_{ij}, $i\neq j\neq k$ and can be assigned according to any of the six permutations of 1, 2, and 3.

APPENDIX II: LONGITUDINAL MAGNETORESISTANCE OF A GENERAL ELLIPSOIDAL ENERGY BAND

The longitudinal magnetoresistance of the band-structure and relaxation-time model discussed in Sec. VI will be calculated for an arbitrary experimental orientation. The electric-current-density and magnetic-flux-density vectors are assumed to be parallel and directed in a general orientation with respect to the principal axes of the energy band. These axes will be called the 1, 2, and 3 axes or directions. The direction cosines of this arbitrary orientation with respect to the 1, 2, and 3 axes will be denoted by γ_1, γ_2, and γ_3, respectively.

When $\mathbf{B}=0$ and $\mathbf{J}\neq 0$, the resulting longitudinal component of the resultant electric field (component of $\mathbf{E}$ parallel to $\mathbf{J}$) is

$$(E^0)_l=J(\gamma_1^2\rho_{11}+\gamma_2^2\rho_{22}+\gamma_3^2\rho_{33}).$$

When $\mathbf{B}\neq 0$ and $\mathbf{J}\neq 0$, Eq. (III.3a) may be used to write:

$$\begin{aligned}E_1=&J\gamma_1(\rho_{11}+\rho_{1111}\gamma_1^2B^2+\rho_{1122}\gamma_2^2B^2+\rho_{1133}\gamma_3^2B^2)\\&+J\gamma_2(\rho_{123}\gamma_3B+2\rho_{1212}\gamma_1\gamma_2B^2)\\&+J\gamma_3(\rho_{132}\gamma_2B+2\rho_{1313}\gamma_1\gamma_3B^2).\end{aligned}$$

Similar equations may be written for E_2 and E_3—the components of the resulting electric field vector along the 2 and 3 axes.

The change in the longitudinal component of the electric field which is caused by the application of the magnetic field is

$$\Delta E=(E)_l-(E^0)_l.$$

Using the above developments,

$$\begin{aligned}\Delta E/JB^2=&(\rho_{1122}+\rho_{2211}+4\rho_{1212})\gamma_1^2\gamma_2^2\\&+(\rho_{1133}+\rho_{3311}+4\rho_{1313})\gamma_1^2\gamma_3^2\\&+(\rho_{2233}+\rho_{3322}+4\rho_{2323})\gamma_2^2\gamma_3^2.\end{aligned}$$

This expression has been simplified by noting that $\rho_{1111}=\rho_{2222}=\rho_{3333}=0$ for this band structure. The Hall coefficients do not appear since $\rho_{ijk}=-\rho_{jik}$ and they cancel in pairs. Also, terms of the form ρ_{ijij} and ρ_{jiji} have been combined since they are equal.

Using the results of Appendix I, Eqs. (A3b) and (A3c), for ρ_{iijj} and ρ_{ijij} and assuming that the relaxation time has a factorable energy dependence (relaxation time of form D of the text) it is seen that if

$$\tau_{ij}(E)=\tau_iF(E)\delta_{ij},$$

then

$$\rho_{1122}=\frac{\tau_3}{pm_{33}}\left[\frac{\langle F(E)^3\rangle}{\langle F(E)\rangle^2}-\frac{\langle F(E)^2\rangle^2}{\langle F(E)\rangle^3}\right],$$

$$\rho_{1122}=\rho_{2211},$$

and

$$\rho_{1212}=-\frac{\tau_3}{2pm_{33}}\left[\frac{\langle F(E)^3\rangle}{\langle F(E)\rangle^2}-\frac{\langle F(E)^2\rangle^2}{\langle F(E)\rangle^3}\right].$$

Hence, $(\rho_{1122}+\rho_{2211}+4\rho_{1212})=0$. In the same way, $(\rho_{1133}+\rho_{3311}+4\rho_{1313})=0$ and $(\rho_{2233}+\rho_{3322}+4\rho_{2323})=0$. Thus, it is seen that the longitudinal magnetoresistance $\Delta E/J$ of a SEP energy band is zero in the limit of low magnetic field strengths. This result holds regardless of the orientation of $\mathbf{B}\|\mathbf{J}$ with respect to the principal axes of the energy band. This result holds if the relaxation time is of form C of the text [a scalar function of energy, $\tau_{ij}=F(E)\delta_{ij}$] or of form D [a diagonal tensor with a factorable energy dependence, $\tau_{ij}=\tau_iF(E)\delta_{ij}$]. However this result will not necessarily be true if the relaxation time has a more complicated form—such as form E [a diagonal tensor with a nonfactorable energy dependence, $\tau_{ij}(E)=\tau_i(E)\delta_{ij}$].

It is easy to show that this result does not hold if the energy band is of the many valley form *and* the valleys do not all have the same relative orientations—that is, the valleys differ by more than just simple translations within the Brillouin zone. As an example, the longitudinal magnetoresistance of n-type silicon is zero only when $\mathbf{B}\|\mathbf{J}$ coincides with one of the principal axes of the cubic unit cell.[29]

[29] E. H. Putley, *The Hall Effect and Related Phenomena* (Butterworths Scientific Publications Ltd., London, 1960), p. 19.